ADVANCES IN ATMOSPHERIC SCIENCES, VOL. 32, NOVEMBER 2015, 1504–1516

# Properties of Cloud and Precipitation over the Tibetan Plateau

WANG Chenghai*[1], SHI Hongxia[1], HU Haolin[1,2], WANG Yi[1], and XI Baike[3]

[1]*Key Laboratory of Arid Climate Change and Disaster Reduction of Gansu Province, College of Atmospheric Sciences, Lanzhou University, Lanzhou* 730000

[2]*Troop* 93212*, The People's Liberation Army, Dalian,* 116200

[3]*Department of Atmospheric Sciences, University of North Dakota,* 4149 *University Ave., Box* 31 9006*, Grand Forks, ND* 58202-9006*, USA*

(Received 14 November 2014; revised 10 April 2015; accepted 15 May 2015)

ABSTRACT

The characteristics of seasonal precipitation over the Tibetan Plateau (TP) were investigated using TRMM (Tropical Rainfall Measuring Mission) precipitation data (3B43). Sensitive regions of summer precipitation interannual variation anomalies were investigated using EOF (empirical orthogonal function) analysis. Furthermore, the profiles of cloud water content (CWC) and precipitable water in different regions and seasons were analyzed using TRMM-3A12 data observed by the TRMM Microwave Imager. Good agreement was found between hydrometeors and precipitation over the eastern and southeastern TP, where water vapor is adequate, while the water vapor amount is not significant over the western and northern TP. Further analysis showed meridional and zonal anomalies of CWC centers in the ascending branch of the Hadley and Walker Circulation, especially over the south and east of the TP. The interannual variation of hydrometeors over the past decade showed a decrease over the southeastern and northwestern TP, along with a corresponding increase over other regions.

**Key words**: cloud liquid water content, cloud ice water content, precipitable liquid water, Tibetan Plateau

**Citation**: Wang, C. H., H. X. Shi, H. L. Hu, Y. Wang, and B. Xi, 2015: Properties of cloud and precipitation over the Tibetan Plateau. *Adv. Atmos. Sci.*, **32**(11), 1504–1516, doi: 10.1007/s00376-015-4254-0.

## 1. Introduction

The unique terrain of the Tibetan Plateau (TP) can lead to a unique spatial distribution of clouds and precipitation. The process of transformation between clouds and precipitation plays an important role in manipulating atmospheric heating profiles and generating plateau-scale uplifting force, which acts as a major forcing for establishing and maintaining the TP monsoon circulation (Kuo and Qian, 1981; Luo and Yanai, 1983, Wang et al., 2012). Based on the vertical extension of deep convective cloud systems(DCSs), for example, the convective precipitation induced by a DCS can heat the entire troposphere, while stratiform precipitation only heats the middle and upper troposphere (Houze, 1997). Latent heat flux (LH) serves as a crucial component in diabatic heating on the TP during summer precipitation (Flohn, 1960; Wu and Zhang, 1998; Duan and Wu, 2005). Summer precipitation over the TP accounts for 60%–70% of the annual total precipitation (Yanai et al., 1992). Liu and Yin (2001) examined summer precipitation by using data from 66 stations over the TP, and suggested that summer precipitation accounts for more than 60% of the total annual precipitation at most stations. Therefore, cumulus convection dominates the heating process to the atmosphere in the eastern TP during the summer months. The main kind of cloud on the TP during daytime is convective and, during nighttime is stratiform (Shimizu et al., 2001; Uyeda et al., 2001; Ueno et al., 2001). The highly developed cumulus during the summer months over the TP is typically accompanied with adequate water vapor (Nitta, 1983; Luo and Yanai, 1984; Yanai and Li, 1994).

Fu et al. (2006) showed precipitation to possess a tower mast over a $5^\circ \times 5^\circ$ box in the center of the TP, in both height–longitude and height–latitude cross sections, and the number of isolated rain cells over the center of the TP to be higher than in surrounding regions. Houze et al. (2007) and Romatschke et al. (2010) showed that convection over the whole TP is weaker than over its southern slope and in the South Asia region.

Li et al. (2008) analyzed the cloud water path by using International Satellite Cloud Climate Project (ISCCP) data and concluded that a significant seasonal variation in the cloud water path over the east of the TP was associated with an increasing trend from 1984 to 2004. Luo et al. (2009) analyzed cloud vertical structures by using CloudSat data, and concluded that the amount of multilayered cloud possesses very strong seasonal variation; in particular, it increases sig-

* Corresponding author: WANG Chenghai
Email: wch@lzu.edu.cn

nificantly from winter to summer in the Indian monsoon region. Bai et al. (2008), using the Tropical Rainfall Measuring Mission (TRMM) Multisatellite Precipitation Analysis data, pointed out significant diurnal variation in summer precipitation over the TP, particularly for convective precipitation over the central TP.

Previous studies have revealed that both cloud and precipitation have regional and seasonal variations over the TP; however, few analyses have focused on the ice/liquid water content in either cloud or precipitation, due to a lack of observations. It is also necessary to investigate the latent heat profiles induced by transformation between phase changes of cloud and precipitation, as well as the long-term variations of these cloud and precipitation properties, with the now 13 years of available TRMM data. Section 2 presents the data and method used for separating the sectors of the TP. Section 3 presents the vertical distributions of the ice/liquid water content of both cloud and precipitation in the different sectors of the TP, and also compares the distribution of each parameter with different areas of the TP. Section 4 illustrates the interannual variation of hydrometeors over the 13 years from 1998 to 2010. Finally, a brief conclusion and recommendations for future work are presented in section 5.

## 2. Data description

The TRMM 3B43 dataset provides the best estimated monthly precipitation in the $\pm 50^\circ$ latitude band from all the following data sources: high-quality microwave, infrared, and rain gauge measurements. The grid spacing of this product is $0.25^\circ \times 0.25^\circ$ and it provides relatively fine resolution when used for highly complex terrain, such as that over the TP. More detailed information on the TRMM products can be obtained from the Goddard Earth Sciences Data and Information Services Center (http://disc.sci.gsfc.nasa.gov/precipitation/documentation/TRMM_README/TRMM_3B43_readme.shtml). Because the orography of the TP is inhomogeneous, the entire TP was divided into five different regions according to the EOF of precipitation (Wang and Guo, 2012; Guo and Wang, 2014). Based on the EOF analysis, the properties of cloud and precipitation in each region were investigated using the TRMM 3A12 dataset, which provides monthly TRMM Microwave Imager (TMI) vertical hydrometeor profiles, such as cloud ice content (CIC), cloud liquid water content (CLWC), precipitation ice content (PIC), precipitation liquid water content (PLWC), and latent heat profiles. The TRMM 3A12 data have a spatial resolution of $0.5^\circ \times 0.5^\circ$ and 14 vertical layers ranging from ground level to 18 km. Because the 3A12 dataset simply comprises the monthly means of 2A12, all the uncertainties will be carried from 2A12. The 2A12 dataset, corresponding to the GRPOF2004 algorithm, used a set of eight cloud-resolving model simulations to create the a priori databases for the Bayesian retrieval scheme. Because of the generic properties of passive remote sensing, the precipitation retrieved by the TMI can be significantly underestimated over highly reflective land surfaces, which can be due to ice/snow cover during winter, and/or due to sharp changes in the elevation of the surface. The TMI algorithm may also miss a significant fraction of lighter, isolated precipitation, or that which forms from warm rain processes. Finally, the vertical wind data were used to investigate the relationship between the properties of hydrometeors and the wind profiles. The wind data were obtained from the National Centers for Environmental Prediction reanalysis for the same time periods as the above two datasets, with a resolution of $2.5^\circ \times 2.5^\circ$.

## 3. Distribution of phases of water-vapor hydrometeors and LH over the TP

### 3.1. *EOF analysis*

Previous studies on precipitation have mostly been based on ground observations and, as a consequence, the results from these studies lack adequate spatial representation. Ground observation stations in this region are located primarily in plain river basins and the eastern TP; there are few observations in the western TP (Chen et al., 2012). In contrast, the TRMM data cover the entire TP, possess high temporal and spatial resolution, and are highly reliable (Shen et al., 2010). Therefore, the TRMM 3B43 and 3A12 datasets were used in this study.

The majority of TP rainfall occurs in summer. Figure 1 presents the summer precipitation (June, July and August) over the TP during 1998–2010. The precipitation amount was less than 100 mm (rate of 1 mm $d^{-1}$) over the western TP, northwestern TP and Qaidam Basin, but was more than 800 mm over the southeastern TP. The precipitation amount decreased from the southeast to the northwest. The distribution of precipitation based on the TRMM data is basically consistent with that of ground observations (Fu et al., 2006). However, it is clear that the TRMM data possess advantages over ground observations in depicting the spatial distribution of precipitation (Fujinami et al., 2005; Fu et al., 2006).

The EOF method was used to assess the temporal and spatial characteristics of summer precipitation. The accumu-

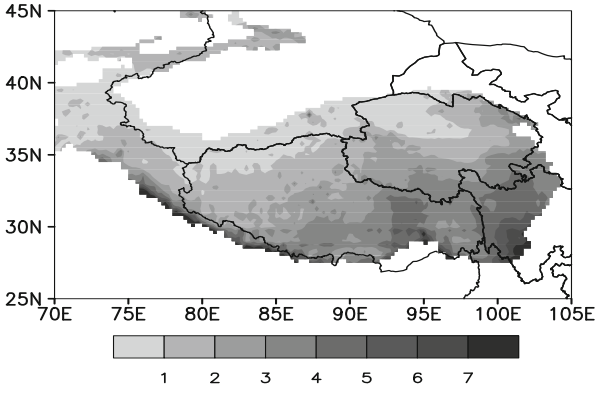


**Fig. 1.** Distributions of summer precipitation (mm $d^{-1}$) on the TP (1998–2010).

lated variance of the first three eigenvectors of precipitation exceeded 73% (Table 1). Thus, the first three eigenvectors are analyzed in this paper.

Figure 2 shows that spatial patterns depicted by the first three eigenvectors are significantly different to each other. Figure 2a shows that the first eigenvector has an explained variance of 34.9% and that the summer precipitation annual anomaly over the south and north of the Tanggula Mountains changes inversely. This reflects the effects of the terrain on precipitation processes.

The second eigenvector of summer precipitation has an explained variance of 23.7% (Fig. 2b). The precipitation anomaly over the eastern and western areas of the TP changes inversely, which is consistent with observations (Fujinami et al., 2005; Fu et al., 2006). Water vapor can barely reach the western regions, which makes the western TP a dry region. This indicates that the precipitation annual anomaly changes inversely between the western TP and the Hengduan Mountains in the east of the Tanggula Mountains. The vapor that moves from the Hengduan Mountains onto the TP only reaches the 90°E region (the source of three rivers). This pattern reflects the transport border for vapor that comes from the Bay of Bengal onto the TP through the valleys of Nujiang River, Lancang River and Jinsha River, the Yangtze River. The third eigenvector accounts for up to 15% of the total variance. This pattern illustrates that the annual anomaly of TP precipitation changes inversely between the central TP (between Mount Kunlun and Gangdisê Range) and the surrounding TP. The central TP is characterized by a dry region that is rich in permafrost, so the precipitation may come from regional water cycles of ice and snow and the permafrost active layer (Duan and Wu, 2005; Wang and Guo, 2012). Based on the above analysis, the TP was divided into five parts (Fig. 3) to investigate the characteristics of precipitation and hydrometeors.

### 3.2. *Distribution of hydrometeors and the relationship with precipitation*

Figure 4 shows the monthly variation of precipitation in the different regions, which illustrates that precipitation over the TP possesses monsoonal features, i.e., rainfall is concentrated during summer, and that large differences exist among the five sub-regions. Region I is far from the influence of the summer monsoon over the Indian peninsula. The precipitation in Region I is much less compared to the other regions, showing little seasonal variation, possibly because of its terrain (Guo and Wang, 2014). The precipitation in the other

**Table 1.** Eigenvectors and their variance of the EOF of summer precipitation (1998–2010).

| Eigenvector | Variance | Accumulating variance |
|---|---|---|
| 1 | 0.349 | 0.349 |
| 2 | 0.237 | 0.586 |
| 3 | 0.145 | 0.731 |
| 4 | 0.07 | 0.801 |
| 5 | 0.036 | 0.837 |
| 6 | 0.024 | 0.866 |
| 7 | 0.024 | 0.89 |
| 8 | 0.018 | 0.908 |

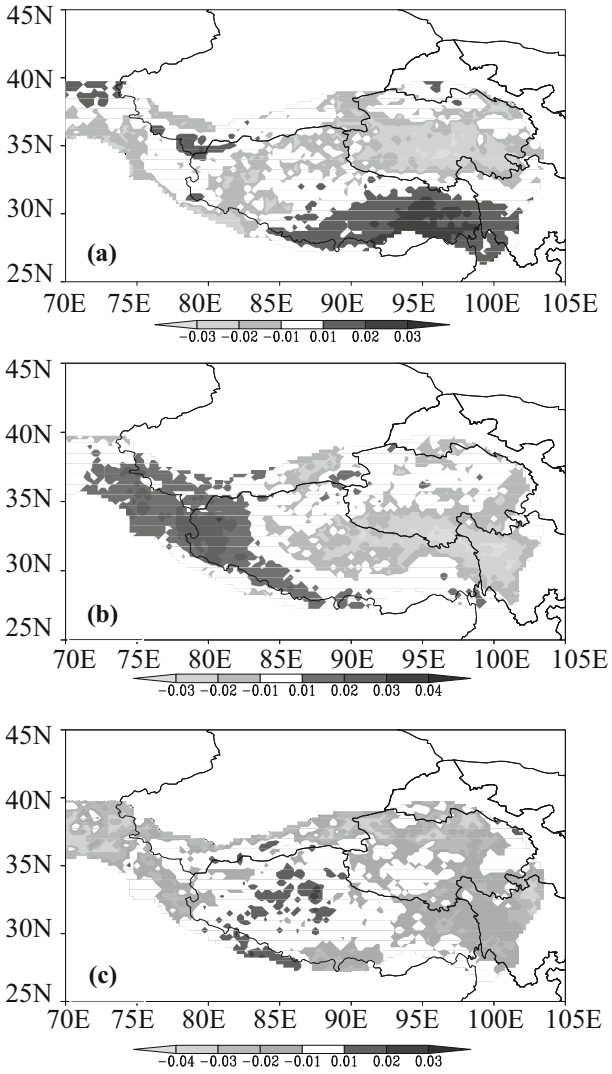


**Fig. 2.** Distribution of the EOF loading vector of TP precipitation in summer from 1998 to 2010: (a) first loading vector; (b) second loading vector; (c) third loading vector.

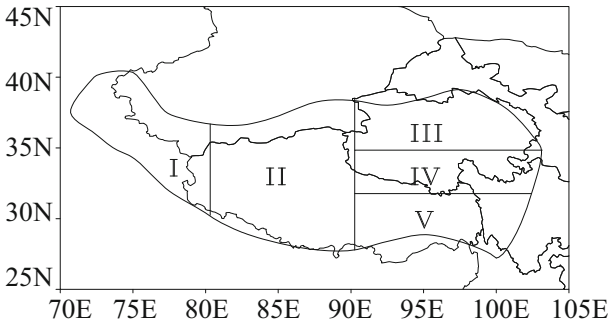


**Fig. 3.** Regions defined by the EOF of summer precipitation in this study.

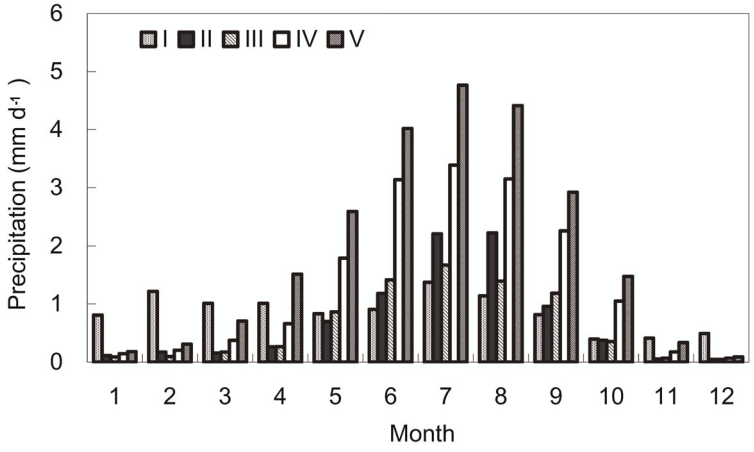


**Fig. 4.** Distribution of monthly TRMM precipitation in five regions of the TP (1998–2010).

four regions peaks in summer. Additionally, the amount of precipitation in Region IV and Region V is significantly greater than that in the other three regions, which can be attributed to the water vapor advected by the South Asian summer monsoon (Goswami, 2005). Specifically, Region V shows the greatest monthly accumulated precipitation over the entire TP, due to the abundant vapor transported by the monsoon. The precipitation amount in Region I and Region III is much lower than in the other three regions because both are influenced the least by the South Asian monsoon (Yeh and Gao, 1979).

The accumulated monthly precipitation is highly unevenly distributed over the TP. The following analyses may explain why the precipitation has such spatial and seasonal variations. First, we analyzed the seasonal CWC (the sum of the CIC and CLWC, Fig. 5), then the precipitable water (PW) (the sum of PLWC and PIC, Fig. 6) and, finally, the LH profiles (Fig. 7), with the aim to elucidate the possible transformation among phases of hydrometeors.

Figure 5 illustrates the seasonal variations of the CWC profiles in the five regions. It is important to note that each diagram in Figs. 5, 6 and 7 has its own starting height, to reflect the average elevation of the region. Region I (Fig. 5a) shows double peaks of CWC in all seasons except winter. The first peak occurs near the lowest plotting height at 4 km, which reflects evaporation from the surface, and the second peak occurs at $\sim$9 km, which represents pure ice water content (Gao et al., 2003). Apparently, the CWC in winter is the lowest among the seasons, and this is either due to a lack of advection toward this region or large retrieval uncertainties over ice/snow-covered surfaces.

Region II (Fig. 5b) has the lowest CWC over the entire year compared to the surrounding regions. Region III (Fig. 5c) also has very low CWC, but we can see the LWC has a peak at around 3 km (near-surface). Region IV and V (Figs. 5d and e) have very similar vertical profiles to each other, and the CWCs in both regions show double peaks, with much higher CWC in Region V than Region IV.

From Fig. 5, it is clear that the maximum CWC happened in different seasons in different regions; specifically, spring in Regions I and V, and autumn in Regions II, III and IV. In Region I, summer shows a very similar CWC vertical distribution as spring, except for lower values at 4 km. Winter shows the lowest CWC in all regions except Region IV, and summer shows the lowest CWC in Region IV. Compared to the lower peaks in all five regions, Region V has the largest CWC and Region II has the lowest CWC. Region I shows a high peak in three seasons and Regions IV and V show very clear high peaks in all four seasons, with the highest in autumn in Region V.

Figure 6 shows the corresponding PW profiles, which is the sum of the PLWC and PIC. The PW decreases with height, which is the same as CWC and changes with height. However, the maximum PW shows different seasonal variations in different regions. In Regions I and II, PW is largest in spring and summer and lowest in winter. In Regions III and IV, PW in spring and autumn is larger than that in summer and winter, and the PW minimum occurs in summer in region IV. In Region V, PW is largest in spring and is lowest in winter, which is similar to the seasonal trend of CLWC. In total, PW in Region V is the largest over the entire TP.

To further analyze the vertical distribution and relationship of CWC and PW, Fig. 7 illustrates the profiles of LH. Similar to CWC and PW, LH decreases with height. The LH is high at near-surface heights; however, unlike the CWC, there is a peak at 9 km in Regions IV and V. It reflects the LH release during the induced condensation of water vapor, and also reveals that the condensation process is more intense than the former. As a result, LH strengthens the convection and, thereby, the LH can reach a greater height, at which the CLWC is smaller .At this height, the liquid water condenses, almost turning into ice crystals. In ice-phase cloud, the LH becomes smaller. In Regions II and III, CWC and PW are at a minimum, which also corresponds to a minimum LH.

Figure 7 shows that LH is relatively large below 8 km. This suggests that water vapor condensation over the TP

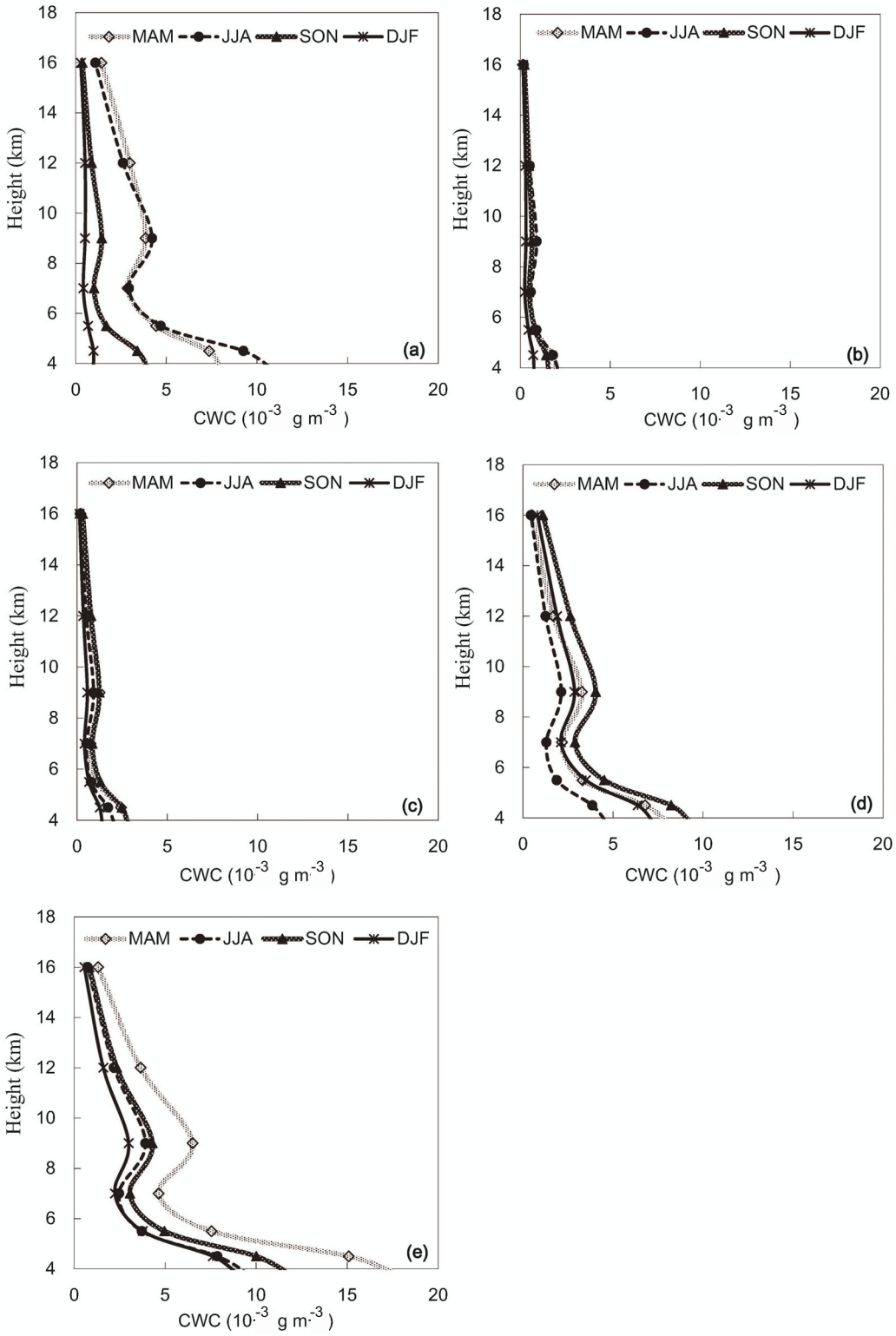


**Fig. 5.** Seasonal Vertical profile of CWC (summation of CLWC and CIC) in five regions ($10^{-3}$ g m$^{-3}$) of the TP from 1998 to 2010: (a) Region I; (b) Region II; (c) Region III; (d) Region IV; (e) Region V.

mainly occurs near the surface, which partly explains the strong convection over the TP caused by diabatic heat near the surface. This is wholly in agreement with Fu et al. (2007). The LH profile of the TP reaches a maximum at around 6–7 km. The LH in Region V is largest over the TP, and is seven to eight times larger than that in Regions II and III. The LH in Regions I and II is nearly the same. The LH maximum is in autumn in Regions III and IV, but in summer in Region V. In all regions except Region IV, the LH in winter is the lowest of the year.

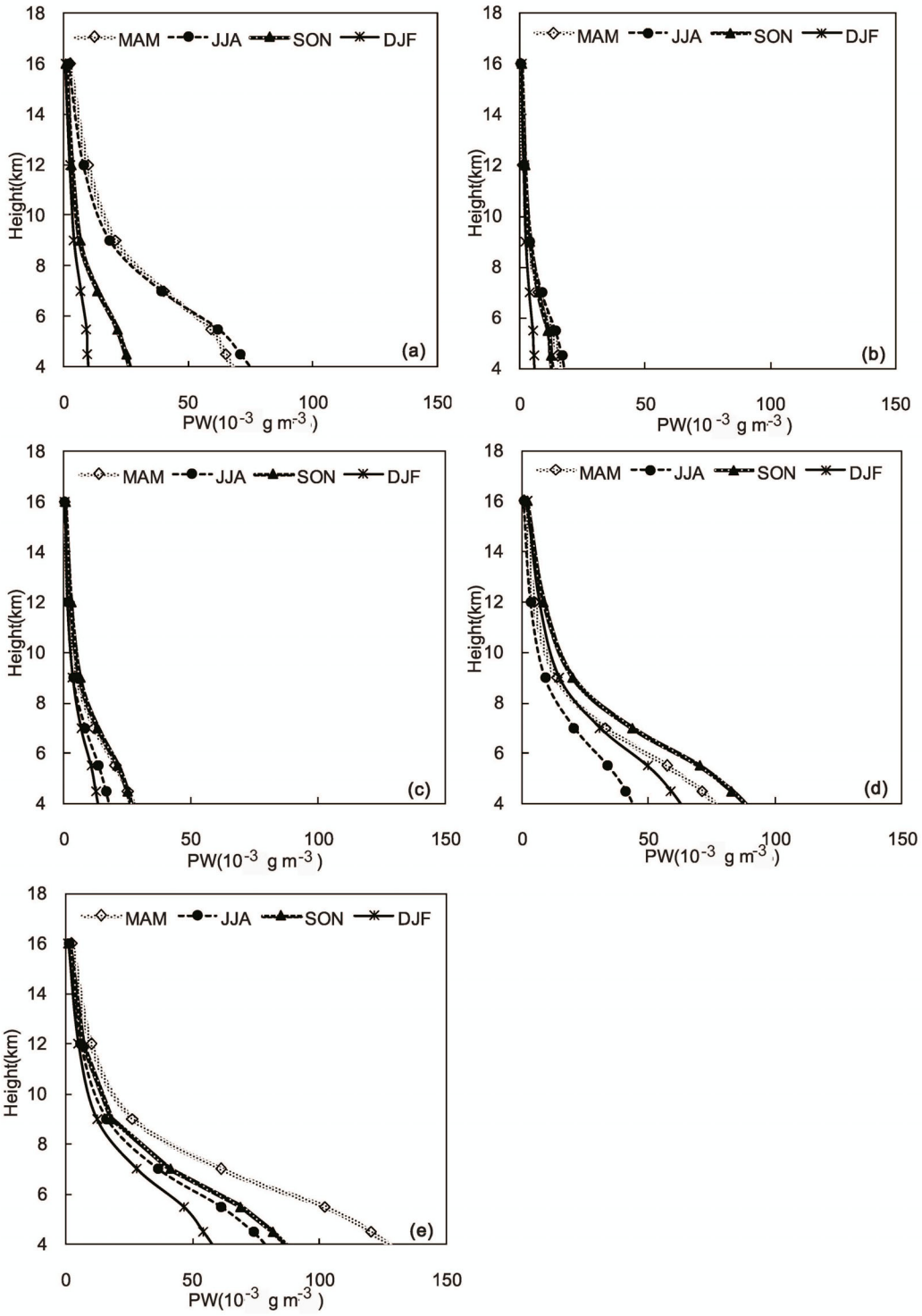


**Fig. 6.** Seasonal vertical profile of PW (summation of PLWC and PIC) ($10^{-3}$ g $m^{-3}$) in five regions of the TP from 1998 to 2010: (a) Region I; (b)Region II; (c) Region III; (d) Region IV; (e) Region V.

As shown in Figs. 5, 6 and 7, the seasonal variations of PW and CWC are almost the same in all regions over the TP, which means that PW and CWC are closely related to each other. The hydrometeors over the eastern and southeastern TP are more abundant, while they are less over the central and northwestern TP. In seasonal terms, the CWC maximum occurs in summer in the western and central TP. Over the eastern TP, the CWC in summer is smaller than that in spring and autumn, especially over the northeastern TP; hydrometeors in summer are less than in winter. This can be attributed to the differences in moisture transportation and weather systems in different seasons. In Region III, where westerly winds prevail, water vapor mainly comes from the westward stream which originated from southern China flows. Considering

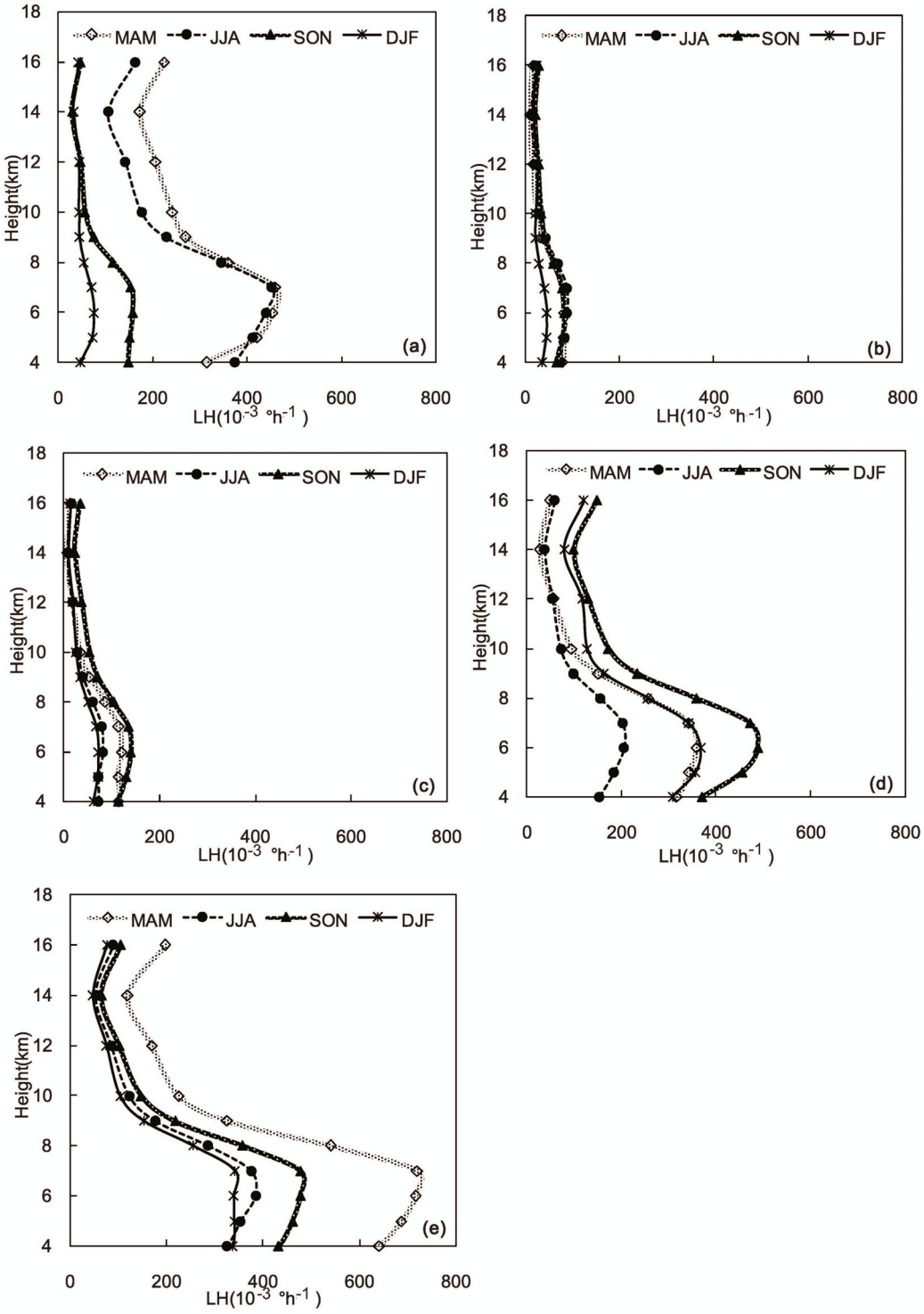


**Fig. 7.** Seasonal vertical profile of LH ($10^{-3}$ °C $h^{-1}$) in five regions of the TP from 1998 to 2010: (a) Region I; (b) Region II; (c) Region III; (d) Region IV; (e) Region V.

that the Qaidam Basin lacks abundant moisture, little precipitation in Region III can be expected.

The 2A12 algorithm cannot provide accurate CLWC and CIC in the mixed-phase region of cloud and precipitation; therefore, the boundary of the CLWC and CIC is unclear. However, regarding the LH profiles in Fig. 7, the LH is larger in Regions IV and V than in the other regions. During the summer half of the year, compared to the winter half, uplift in Regions IV and V is stronger than in the other regions. Therefore, the profile distribution of PW and CWC may be rational, except for some disparity in values.

In general, the CLWC and PW should not equal precipi-

tation. To discuss the relationship between hydrometeors and precipitation, the correlation coefficients between precipitation and a selection of variables—CIC, CLWC, CWC, PIC, PLWC and PW—were calculated. The hydrometeor content was defined as the summation of all hydrometeors in a unit area:

$$p = \sum_{i=1}^{14} w_i H_i \ . \tag{1}$$

Here, $p$ is the hydrometeor path (g m$^{-2}$), $w_i$ is the content of each hydrometeor in a specific level (g m$^{-3}$), and $H_i$ is the thickness of each level.

There is a complex link between summer hydrometeor and precipitation values (Table 2). Precipitation is rare in Regions I and III. In Region I in particular, the precipitation amount is small, and monthly precipitation changes are small within a year, i.e., monsoonal characteristicsare less obvious.Thus, the correlation between hydrometeors and precipitation is poor. Region III is located in the northeastern TP and is controlled by westerly winds rather than the monsoon, meaning that the correlation here is also weak. This could be attributed to the fact that there is little water vapor advected in Regions I and III, where precipitation mainly comes from the regional recycling of vapor (Wang and Guo, 2012). In addition, the satellite data resolutions are low, meaning they are unable to capture showery precipitation. In the other three regions, the correlation between CIC and precipitation is significant; however, the CLWC is only significantly correlated with precipitation in Regions II and V. In the eastern TP, the PWC and PIC are both correlated with precipitation significantly. A key feature is that, south of the Three Rivers (Yangtze River, Yellow River and Lantsang River) Source, precipitation is closely related to the CIC and PW, and the effect of orographic lift is notable. In Region IV (the Tanggula Mountains), no significant correlation exists between precipitation and CLWC or CWC. The cloud type over this region is mainly high cloud, in which ice prevails. As a result, the correlation between precipitation and CIC is significant. In the western and northeastern TP, where vapor is not readily available, the precipitation amount is small and related poorly to hydrometeors. This may be caused by two reasons: (1) the accuracy of the retrieving algorithm is limited and (2) precipitation is mainly derived from regional water recycling.

Additionally, not all CWC results in precipitation, and different types of cloud have various water amounts. It should be noted that the formation of precipitation from clouds is a dynamic process, so hydrometeors can only partly reflect precipitation, which results in a poor correlation between precipitation and hydrometeors.

### 3.3. *Spatial and temporal distribution characteristics of different hydrometeors*

To further discuss the spatial and temporal distributions of each hydrometeor type and the corresponding influencing factors, the zonal and meridional distributions of hydrometeors are presented in Figs. 8 and 9.

Figure 8 illustrates the anomalies of the zonal vertical distribution of hydrometeors, LH and vertical circulations along 30°–37.5°N and 5°S–5°N. In the northern midlatitudes, there is a large-value region of hydrometeors (positive anomaly) within 120°–160°E (Fig. 8a). In this area, there also exists a maximum center of CIC, and the center corresponds to the upward branch of vertical circulation over the western Pacific. To the east and west of the TP, the heights of CWC are apparently different to that over the TP. In the equatorial region, two maximum centers exist within 60°–100°E and 120°–160°E, respectively, which both correspond to the upward branch of Walker Circulation (Fig. 8d). There is a minimum center within 160°–80°W, and this corresponds to the downward branch of Walker Circulation. It can also be seen that there is Walker-like circulation in the midlatitudes of the Northern Hemisphere.

In Figures 8b and e, over the midlatitudes in the Northern Hemisphere, PW in the Western Hemisphere is notably larger than that in the Eastern Hemisphere. There is a positive anomaly center of PW over the western Pacific, and PW over the TP is larger than that of other regions within the same latitude. Over the west of the TP, there is a weak negative anomaly center. Similarly, a positive anomaly center of PW is found on the upward branch of the Walker circulation. Comparatively, in the equatorial region, the zonal negative anomaly center of the PW and CWC is also found in the east of the Pacific.

Studies show that, during the summer, the TP can also be a heat source (Flohn, 1957; Yeh et al., 1957), which creates convection and a large amount of cloud due to large-scale upward motion. There is a positive anomaly of LH in the upper troposphere over the central Pacific. The center of the positive anomaly is at the top of the upward motion. At the same levels, there are negative anomalies of LH centers in

**Table 2.** Correlation between hydrometeors and precipitation in summer over the TP (1998–2010). A single asterisk (*) indicates statistical significance at the 90% confidence level; a double asterisk (**), 95%.

| Region | Cloud ice content | Cloud liquid water content | Cloud water (cloudiness + cloud liquid) | Precipitable ice content | Precipitable liquid water content | Precipitable water |
|---|---|---|---|---|---|---|
| I | 0.0812 | 0.0768 | 0.0825 | 0.0707 | 0.0883 | 0.0775 |
| II | 0.4900* | 0.6210** | 0.6463** | 0.3432 | 0.5260* | 0.4048 |
| III | 0.2715 | 0.3723 | 0.3450 | 0.2993 | 0.0412 | 0.2202 |
| IV | 0.4418* | 0.1830 | 0.2835 | 0.7942** | 0.6682** | 0.7644** |
| V | 0.7630** | 0.7429** | 0.7570** | 0.5399* | 0.6478** | 0.5972** |
| QXP | 0.3816 | 0.3696 | 0.4053 | 0.2744 | 0.3715 | 0.3127 |

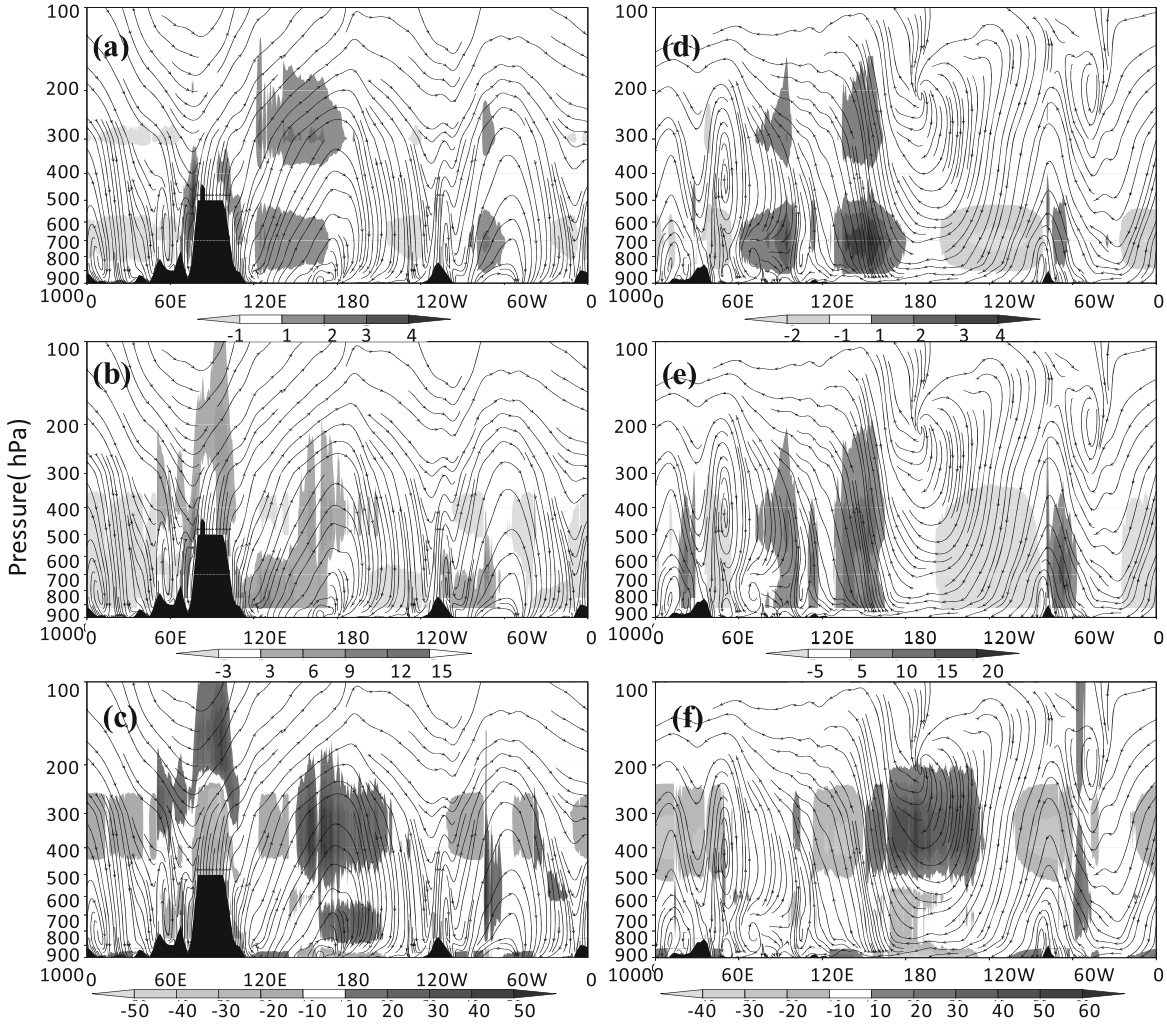


**Fig. 8.** Longitude–altitude cross section and distribution of hydrometeor anomalies, LH and circulation ($\omega \times 1000$). Shading is the hydrometeor longitude anomalies ($10^{-3}$ g m$^{-3}$) and LH ($10^{-3}$ °C h$^{-1}$) (30°–37.5°N) in summer: (a) CWC; (b) PW; (c) LH (5°S–5°N); (d) CWC; (e) PW; (f) LH.

other regions. However, in the lower level over the TP, there is a negative anomaly center of LH; the temperature is lower compared to that in other regions in the same latitude. In the upper troposphere over the TP, there is a large positive anomaly center of LH, which corresponds to the PW positive anomaly center, as well as to the upward motion. The negative and positive anomaly of LH separates at the boundary between CIC and the CLWC, which is with the drag of vertical motion. The ascending vapor condenses and heats the atmosphere. In the anomaly centers of PW, CLWC and CIC are consistent in two latitude cross profiles. However, these are different from the situation over the TP and its adjacent regions. Over the western Pacific, PW is mainly from the CLWC, but over the eastern Pacific, it is mainly from the higher CLWC transforming into CIC.

In order to analyze the special characteristics of hydrometeors in temporal and spatial distributions over the TP, Fig. 9 illustrates the meridional distribution anomalies and vertical circulations of hydrometeors and LH between 40°S and 40°N. In Fig. 9a, the TP causes an extension of the upward branch of the Hadley Circulation stretching to the south of the TP. In the upward branch of the Hadley Circulation, the meridional positive anomaly center of CLWC and CIC is within 10°–20°N. Similarly, negative anomalies of hydrometeor centers are found in the downward motion area of the Hadley Circulation in the Southern Hemisphere. Over the southern slope of the TP, there is an upward motion area of monsoon circulation, and there is another maximum center of CWC. It should be noted that this center is mainly vapor condensation caused by the orographic lifting effect; hence, it is not the CIC center anomaly. In a similar way, there is a negative anomaly center of hydrometeors over the northern slope of the TP—an arid atmosphere center in north slope of the TP, which is caused by the water vapor condensing and dropping in south slope because of terrain lifting. This is consistent with the spatial structure of the CLWC and CIC over Regions IV and V. Figure 9b presents the PW spatial structure. Apparently, positive and negative anomalies of hydrometeors are

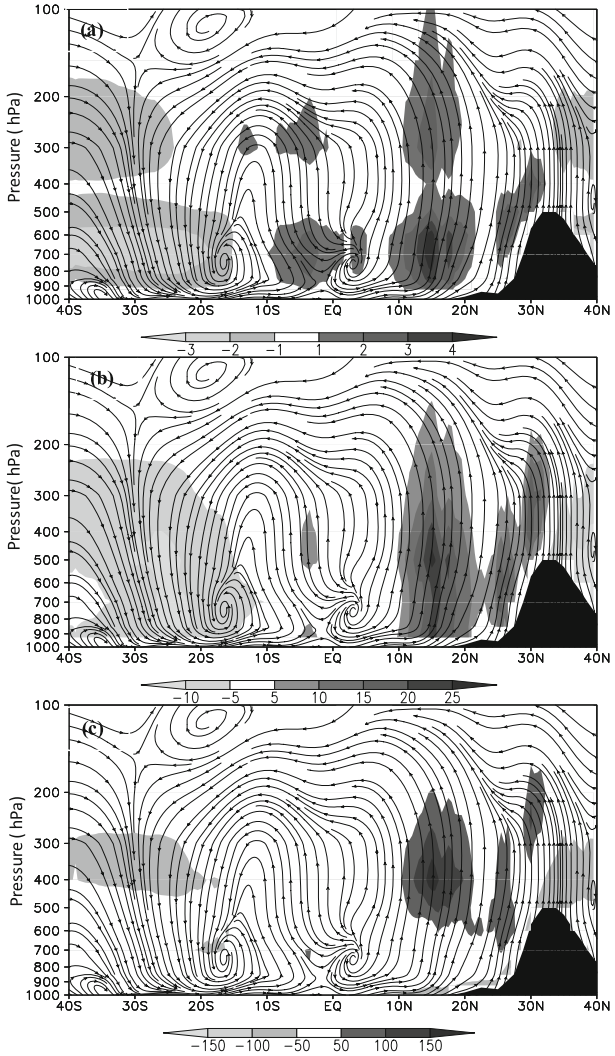


**Fig. 9.** Latitude–altitude crosssection and distribution of hydrometeor anomalies, LH and circulation ($\omega \times 1000$). Shading is hydrometeor latitude anomalies ($10^{-3}$ g m$^{-3}$) and LH ($10^{-3}$ °C h$^{-1}$) in summer (90°–100°E): (a) CWC; (b) PW; (c) LH.

centered in the upward and downward motion areas of the Hadley Circulation, respectively. Because of the existence of the TP, the positive anomaly center of hydrometeors in the Northern Hemisphere is found to be mainly located over the southern TP, while the negative anomaly center is over the northern TP. The positive anomaly center of hydrometeorsis consistent with the CWC values in Fig. 8a. The LH has the same spatial structure as the hydrometeors. In the hydrometeor profiles within 10°–20°N, a positive anomaly of LH is centered on 400 hPa, where the boundary between CLWC and CIC is located. The LH over the southern TP reflects the lifting force that condenses water vapor. The negative anomaly center of LH over the northernTP is related to surface evaporation.

By analyzing Figs. 8 and 9, it can be seen that the lifting and condensation effect makes the southern and eastern TP two positive anomaly centers of hydrometeors. On the one hand, the hydrometeor center is located on the ascending branch of the Hadley and Walker Circulation, because there is abundant vapor in the monsoon trough in the Bay of Bengal, which is located south of the TP, and the hydrometeors are the product of water vapor and upward motion; while on the other hand, the vapor condenses, releasing LH to reinforce the upward motion of the Hadley and Walker Circulation, which is more significant over the southern and southeastern TP. Additionally, the regional water cycling induced by evaporation is also an important process in the formation of cloud and precipitation.

## 4. Interannual variation of hydrometeors in the past decade

In the past decade, the globe has steadily been warming. The warming of the TP is notable, especially in the sense that the minimum air temperature is increasing faster than the maximum air temperature (Karl et al., 1991; Easterling et al., 1997). Meanwhile, the precipitation is changing in different ways in different regions over the TP (Wang and Guo, 2012). The rising temperature and the changes in precipitation will inevitably change the evaporation and regional water cycles. In order to illustrate the changes in hydrometeors, variations of standardized values of summer hydrometeors and precipitation during 1998 to 2010 are presented in Fig. 10. These change patterns of different hydrometeors are in general the same in all analyzed regions, probably caused by the retrieval algorithm of the satellite data. Hydrometeors over Regions I, II, and IV increased in the past decade and decreased over Regions III and V, while precipitation increased in all regions except Region V. The change patterns of precipitation and hydrometeors are not consistent, even being of opposite phase in Regions II and III (Figs. 10b and c), which are the extremely arid regions. With the increase in regional precipitation, this relevance between precipitation and hydrometeors becomes better, especially in Region V. Precipitation in Region V of the TP was most abundant. The analysis in section 3.2 (of the results in Table 2) can also explain the poor correlation of the interannual variability between hydrometeors and precipitation in extremely arid regions. This variation in Fig. 10 is consistent with the change in water vapor over the whole TP. A possible explanation of such consistency is the regression of the South Asian Monsoon in the last decade (Wang, 2001). The regression of the South Asian Monsoon would lead to a decrease in the amount of water vapor that could be transported onto the TP. The precipitation and hydrometeors would first decrease over Region V. A change in hydrometeors would also happenin Region III, which would also be affected by the monsoon. The amount of water vapor advecting into Regions I and II was small, which is mainly regionally recycled and would thus not have been affected by the monsoon regression. There are several lakes and river basins in Region IV and, as a result, hydrometeors over this region mainly derived from increased evaporation accompanying the temperature increase. However, this result needs further investigation.

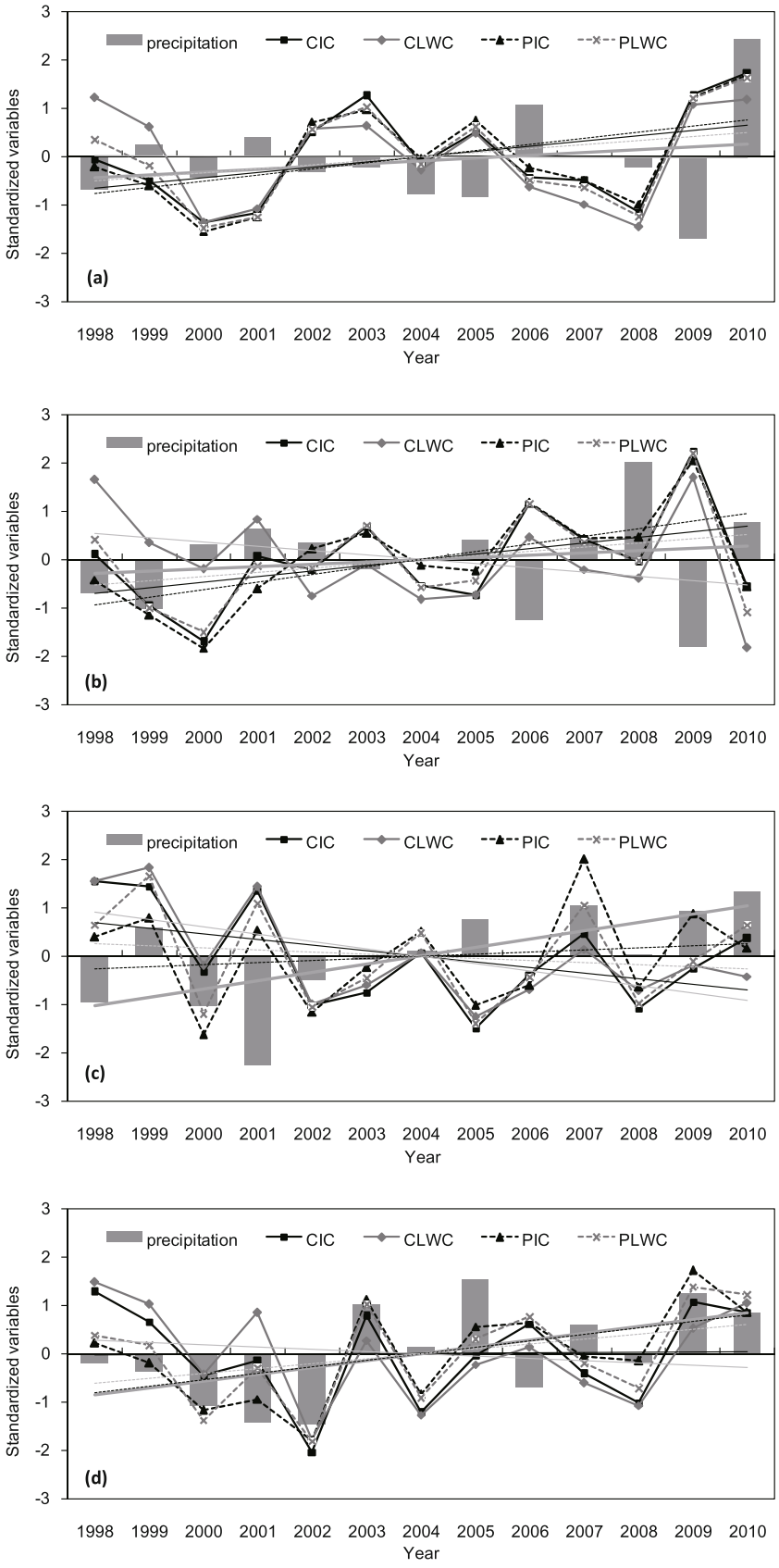


**Fig. 10.** Interannual variability of summer hydrometeors and precipitation over the TP from 1998 to 2010: (a) Region I; (b) Region II; (c) Region III; (d) Region IV; (e) Region V.

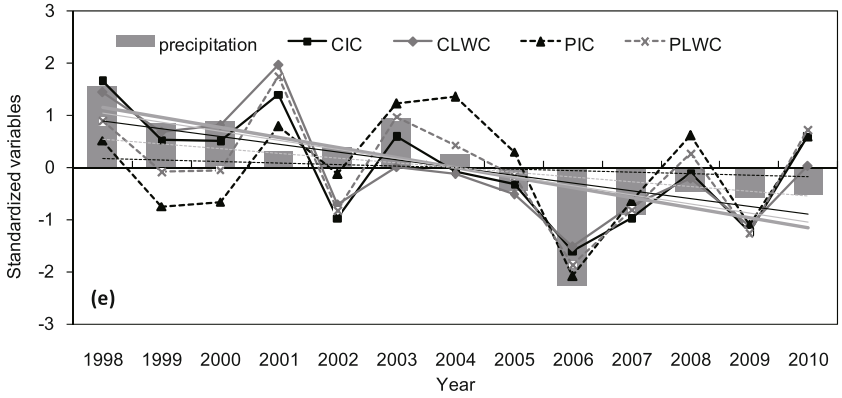


**Fig. 10.** (Continued.)

## 5. Conclusion

The temporal and spatial characteristics of hydrometeors over the TP, as well as the interactions between cloud and precipitation, were analyzed. Clearly, TRMM precipitation data can shed light on the temporal and spatial structure of summer precipitation over the TP. Specifically, it was found that the amount of precipitation decreases from the southeastern to the northwestern TP. The annual precipitation anomalies over the southern and northern Tanggula Mountains change inversely, as do the annual precipitation anomalies over the east and west of 85°E, as determined by EOF analysis. The climate diversity over the TP is notable, and such diversity is mainly caused by the mountainous terrain. The western TP rarely receives water vapor from the southeast. Thus, any precipitation observed in this area is a result of non-monsoonal processes.

The seasonal variation of hydrometeors is significant over TP. Hydrometeors in atmosphere are adequate over the southeastern TP and inadequate over the central TP and northeastern TP. Over the western TP and central TP, the annual hydrometeors peak during the summer. However, over the three regions in the eastern TP (Regions III, IV and V), hydrometeors in summer are less abundant than in spring and autumn. All hydrometeor types are closely related to the upward motion of the atmospheric circulation. The vertical motion takes considerable responsibility for the formation of hydrometeors.

CWC at 6–8 km is the lowest. This height is also the transition height of cloud liquid water to cloud ice water; theoretically, this height should be the maximum of LH. It is worth pointing out that the TMI sounding error must be considered. In addition, the 3A12 precipitation retrievals are based on ice scattering signatures aloft; this paper focuses on the relationship of precipitation and CWC. Also, in general, in the lower level, the major CWC is liquid. The analysis of the annual cycle of precipitation will be affected by the sensitivity of rainfall retrievals in cold-season precipitation. However, the precipitation over the TP mainly occurs in summer, which can partly avoid this shortcoming. It is also the best way for a deep understanding of the distribution and relationship of precipitation and hydrometeors. Liu and Fu (2007a) compared the differences between precipitation datasets of TMI and Global Precipitation Climatology Project data.They proposed that the increased ice particles in upper deep convection systems may lead to an overestimation of precipitation overthe TP, which is attributable to the TMI terrestrial algorithm relying on the scattering signal from ice particles (Fu and Liu, 2007; Fu et al., 2007); plus, TMI signals contains radiation information from both precipitation and the land surface (Fu et al., 2007; Liu and Fu, 2007b).

In the past decade, hydrometeors have decreased over the southeastern and northeastern TP. The decreasing trend over the southeastern TP may have been affected by the regression of the South Asian Monsoon. Hydrometeors over the western TP and the north of the Tanggula Mountains have generally increased. Such changes are consistent with the change in precipitation where water vapor is adequate, reflecting a regional reaction to global warming.

***Acknowledgements.*** This work was supported by the National Key Basic Research Program of China (2013CBA01808), National Natural Science Foundation of China (Grant Nos. 91437217, 41275061, and 41440035). The TRMM data used in this study were processed by the TRMM Science Data and Information System and the TRMM Office, and the data were downloaded from the Goddard Distributed Active Archive Center. Special thanks are given to the supercomputing environment of Gansu Province Supercomputer Center for providing an effective computing environment.

### REFERENCES

Bai, A., C. H. Liu, and X. D. Liu, 2008: Diurnal variation of summer rainfall over the Tibetan Plateau and its neighboring regions revealed by TRMM Multi-satellite Precipitation Analysis. *Chinese Journal of Geophysics*, **51**(3), 704–714. (in Chinese)

Chen, H. M., W. H. Yuan, J. Li, and R. C. Yu, 2012: A possible cause for different diurnal variations of warm season rainfall as shown in station observations and TRMM 3B42 data over the southeastern Tibetan Plateau. *Adv. Atmos. Sci.*, **29**, 193–200, doi: 10.1007/s00376-011-0218-1.

Duan, A. M., and G. X. Wu, 2005: Role of the Tibetan Plateau thermal forcing in the summer climate patterns over subtropical Asia. *Climate Dyn.*, **24**(7–8), 793–807.

Easterling, D. R., and Coauthors, 1997: Maximum and minimum temperature trends for the globe. *Science*, **277**(5324), 364–

367.

Flohn, H., 1957: Large scale aspects of the "summer monsoon" in South and East Asia. *J. Meteor. Soc. Japan*, **75**, 180–186.

Flohn, H., 1960: Recent investigation on the mechanism of the "summer monsoon" of southern and eastern Asia. *Proc. Symp. Monsoon of the World*, New Delhi, Hindu Union Press, 75–88.

Fu, Y. F., and G. S. Liu, 2007: Possible misidentification of rain type by TRMM PR over Tibetan Plateau. *Journal of Applied Meteorology and Climatology*, **46**(5), 667–672.

Fu, Y. F., G. S. Liu, G. X. Wu, R. C. Yu, Y. P. Xu, Y. Wang, R. Li, and Q. Liu, 2006: Tower mast of precipitation over the central Tibetan Plateau summer. *Geophys. Res. Lett.*, **33**, L05802, doi: 10.1029/2005GL024713.

Fu, Y. F., D. Liu, Y. Wang, R. C. Yu, Y. P. Xu, and R. Chen, 2007: Characteristics of precipitating and non-precipitating clouds in typhoon Ranan as viewed by TRMM combined measurements. *Acta Meteorologica Sinica*, **65**(3), 316–328 (in Chinese).

Fujinami, H., S. Nomura, and T. Yasunari, 2005: Characteristics of diurnal variations in convection and precipitation over the southern Tibetan Plateau during summer. *SOLA*, **1**, 49–52.

Gao, B. C., P. Yang, G. Guo, S. K. Park, W. J. Wiscombe, and B. D. Chen, 2003: Measurements of water vapor and high clouds over the Tibetan Plateau with the Terra MODIS instrument. *IEEE Transactions on Geoscience and Remote Sensing*, **41**(4), 895–900.

Goswami, B. N., 2005: South Asian monsoon. *Intraseasonal Variability in the Atmosphere-Ocean Climate System*, Springer, Berlin Heidelberg, 19–61.

Guo, Y. P., and C. H. Wang, 2014: Trends in precipitation recycling over the Qinghai-Xizang Plateau in last decades. *J. Hydrol.*, **517**, 826–835, doi: 10.1016/j.jhydrol.2014.06.006.

Houze, R. A., Jr., 1997: Stratiform precipitation in regions of convection: A meteorological paradox? *Bull. Amer. Meteor. Soc.*, **78**(10), 2179–2196.

Houze, R. A. Jr., D. C. Wilton, and B. F. Smull, 2007: Monsoon convection in the Himalayan region as seen by the TRMM Precipitation Radar. *Quart. J. Roy. Meteor. Soc.*, **133**, 1389–1411.

Karl, T. R., G. Kukla, V. N. Razuvayev, M. J. Changery, R. G. Quayle, R. R. Heim Jr., D. R. Easterling, and C. B. Fu, 1991: Global warming: Evidence for asymmetric diurnal temperature change. *Geophys. Res. Lett.*, **18**(12), 2253–2256.

Kuo, H. L., and Y. F. Qian, 1981: Influence of the Tibetan Plateau on cumulative and diurnal changes of weather and climate in summer. *Mon. Wea. Rev.*, **109**(11), 2337–2356.

Li, X. Y., X. Guo, and J. Zhu, 2008: Climatic distribution features and trends of cloud water resources over China. *Chinese J. Atmos. Sci.*, **32**(5), 1094–1106, doi: 10.3878/j.issn.1006-9895.2008.05.09. (in Chinese).

Liu, Q., and Y. F. Fu, 2007a: An examination of summer precipitation over Asia based on TRMM/TMI. *Science in China* (*D*), **50**, 3430–441.

Liu, Q., and Y. F. Fu, 2007b: Characteristics of latent heating over the Tibetan Plateau during summer. *Journal of University of Science and Technology of China*, **37**(3), 303–309.

Liu, X. D., and Z. Y. Yin, 2001: Spatial and temporal variation of summer precipitation over the eastern Tibetan Plateau and the North Atlantic Oscillation. *J. Climate*, **14**(13), 2896–2909.

Luo, H. B., and M. Yanai, 1983: The large-scale circulation and heat sources over the Tibetan Plateau and surrounding areas during the early summer of 1979. Part I: Precipitation and kinematic analyses. *Mon. Wea. Rev.*, **111**(5), 922–944.

Luo, H. B., and M. Yanai, 1984: The large-scale circulation and heat sources over the Tibetan Plateau and surrounding areas during the early summer of 1979. Part II: Heat and moisture budgets. *Mon. Wea. Rev.*, **112**(5), 966–989.

Luo, Y. L., R. H. Zhang, and H. Wang, 2009: Comparing occurrences and vertical structures of hydrometeors between eastern China and the Indian monsoon region using CloudSat/CALIPSO data. *J. Climate*, **22**, 1052–1064.

Nitta, T., 1983: Observational study of heat sources over the eastern Tibetan Plateau during the summer monsoon. *J. Meteor. Soc. Japan*, **61**(4), 590–605.

Romatschke, U., S. Medina, and R. A. Houze Jr., 2010: Regional, seasonal, and diurnal variations of extreme convection in the South Asian region. *J. Climate*, **23**, 419–439.

Shen, Y., A. Y. Xiong, Y. Wang, and P. P. Xie, 2010: Performance of high-resolution satellite precipitation products over China. *J. Geophys. Res.*, **115**, D02114, doi: 10.1029/2009JD012097.

Shimizu, S., K. Ueno, H. Fujii, H. Yamada, R. Shirooka, and L. P. Liu, 2001: Mesoscale characteristics and structures of stratiform precipitation on the Tibetan Plateau. *J. Meteor. Soc. Japan*, **79**(1B), 435–461.

Ueno, K., H. Fujii, H. Yamada, and L. P. Liu, 2001: Weak and frequent monsoon precipitation over the Tibetan Plateau. *J. Meteor. Soc. Japan*, **79**(1B), 419–434.

Uyeda, H., and Coauthors, 2001: Characteristics of convective clouds observed by a Doppler radar at Naqu on Tibetan Plateau during the GAME-Tibet IOP. *J. Meteor. Soc. Japan*, **79**(1B), 463–474.

Wang, C. H., and Y. P. Guo, 2012: Precipitable water conversion rates over the Qinghai-Xizang (Tibet) Plateau: Changing characteristics with global warming. *Hydrological Processes*, **26**(10), 1509–1516.

Wang, C. H., L. Yu, and B. Huang, 2012: The impact of warm pool SST and general circulation on increased temperature over the Tibetan Plateau. *Adv. Atmos. Sci.*, **29**(2), 274–284, doi: 10.1007/s00376-011-1034-3.

Wang, H. J., 2001: The weakening of the Asian monsoon circulation after the end of 1970's. *Adv. Atmos. Sci.*, **18**(3), 376–386, doi: 10.1007/BF02919316.

Wu, G. X., and Y. S. Zhang, 1998: Tibetan Plateau forcing and the timing of the monsoon onset over South Asia and the South China Sea. *Mon. Wea. Rev.*, **126**, 913–927.

Yanai, M., and C. F. Li, 1994: Mechanism of heating and the boundary layer over the Tibetan Plateau. *Mon. Wea. Rev.*, **122**(2), 305–323.

Yanai, M., C. F. Li, and Z. S. Song, 1992: Seasonal heating of the Tibetan Plateau and its effects on the evolution of the Asian summer monsoon. *J. Meteor. Soc. Japan*, **70**(1B), 319–351.

Yeh, T.-C., S.-W. Lo, and P.-C.Chu, 1957: The wind structure and heat balance in the lower troposphere over Tibet Plateau and its surrounding. *Acta Meteorological Sinica*, **28**(2), 108–121 (in Chinese with English Abstract).

Yeh, T. C., and Y. X. Gao, 1979: *The Meteorology of the Qinghai-Xizang* (*Tibet*) *Plateau*. Science Press, Beijing, 278 pp. (in Chinese)